

Figure 1: The Coxcomb of visual results and key evaluation metrics. Our SNN-based method transfers the knowledge from the ANNs for better image restoration performance.

BRIDGE THE GAP BETWEEN SNN AND ANN FOR IMAGE RESTORATION

Xin Su

Fuzhou University
suxin4726@gmail.com

Chen Wu

University of Science and Technology of China
wuchen5x@mail.ustc.edu.cn

Zhuoran Zheng*

Sun Yat-sen University
zhengzrz@just.edu.cn

ABSTRACT

Models of dense prediction based on traditional Artificial Neural Networks (ANNs) require a lot of energy, especially for image restoration tasks. Currently, neural networks based on the SNN (Spiking Neural Network) framework are beginning to make their mark in the field of image restoration, especially as they typically use less than 10% of the energy of ANNs with the same architecture. However, training an SNN is much more expensive than training an ANN, due to the use of the heuristic gradient descent strategy. In other words, the process of SNN's potential membrane signal changing from sparse to dense is very slow, which affects the convergence of the whole model. To tackle this problem, we propose a novel distillation technique, called asymmetric framework (ANN-SNN) distillation, in which the teacher is an ANN and the student is an SNN. Specifically, we leverage the intermediate features (feature maps) learned by the ANN as hints to guide the training process of the SNN. This approach not only accelerates the convergence of the SNN but also improves its final performance, effectively bridging the gap between the efficiency of the SNN and the superior learning capabilities of ANN. Extensive experimental results show that our designed SNN-based image restoration model, which has only 1/300 the number of parameters of the teacher network and 1/50 the energy consumption of the teacher network, is as good as the teacher network in some denoising tasks.

* * Corresponding author

1 INTRODUCTION

Image restoration, a classical research area in computer vision, focuses on recovering high-quality images from degraded observations. Most existing frameworks for image restoration use artificial neural networks (ANNs), which have high performance but also often rely on large-capacity models to achieve optimal performance. For instance, Restormer [48] and PromptIR [30] networks have 26.10M and 35.59M parameters, respectively, making them unsuitable for deployment on edge devices. The growing importance of devices with low power or battery constraints in various real-world applications, such as spiking neural networks (SNNs) offers a promising alternative [2, 6, 16, 36, 40, 41].

SNNs utilize binary signals (spikes) instead of continuous signals for neuron communication, reducing data transfer and storage overhead. Moreover, Spiking Neural Networks (SNNs) feature asynchronous processing and event-driven communication, which can eliminate redundant computations and synchronization burdens. When implemented in neuromorphic hardware, as mentioned in [26, 29], SNNs demonstrate exceptional energy efficiency.

Unfortunately, in the challenging domain of image restoration, there is a notable absence of an SNN-based benchmark that can achieve performance levels comparable to those of its ANN counterpart. This is largely due to the slow training process of SNNs, which, relying on spike-based signaling, require extensive data exposure to generate predictions that match the accuracy of ANNs. This reliance on prolonged data exposure is particularly problematic when it comes to the extraction of subtle information from images that are visually redundant, as the training process becomes even more time-consuming.

In recent years, knowledge distillation as a promising approach for training heterogeneous models for knowledge transfer [11, 24, 28]. These efforts have piqued our curiosity, prompting us to explore the question: *Is it feasible to transfer knowledge from ANNs to SNNs effectively?* Xu et al. [44] presented a case of ANN-SNN distillation, in which the SNN retained 90% of the performance of the ANN while consuming less power. In this paper, our objective is to address the prolonged training times in SNNs by leveraging the exceptional performance capabilities of ANNs to enhance and expedite the capabilities of SNNs. We propose a novel approach to train a thin SNN, called **H-KD**, which facilitates the distillation of knowledge in the feature space directly from ANNs. Specifically, we propose an efficient and effective SNN-based method, called **SpikerIR**, to solve the image restoration problem. This method aligns the representations from the ANN’s decoder with those from our proposed SNN architecture, ensuring that the knowledge transferred is accurate information. Furthermore, considering that heterogeneous models may learn distinct predictive distributions due to their different inductive biases, we utilize the surrogate gradients to mitigate failure to surpass the performance of the original network (ANNs). Compared to other ANN-based deraining models, our method can gain better performance with shorter time steps. We consider the five different degradation types, as shown in Figure 1, helping produce visually appealing results across the different degradations. Our main contributions are summarised as follows:

- (1) We present SpikerIR, the first general image restoration SNN-based method to the best of our knowledge with a minimal parameter count of only **0.07M**, perfectly tailored for real-world applications on resource-limited devices.
- (2) We design a scheme, called H-KD, to accelerate the SNNs training process, by distilling the knowledge from the ANN to obtain comparable performance for image restoration. Extensive experimental results on unified image restoration display that our proposed model can obtain excellent performance in a shorter time while reducing energy costs.

2 RELATED WORK

Image Restoration. Image restoration [42] focuses on reconstructing a degraded image to produce a high-quality version, addressing a core challenge in computer vision. This encompasses a range of tasks, including image denoising [51, 52], deraining [14, 33], dehazing [31, 34], and motion deblurring [5, 7] etc. Although these methods demonstrate remarkable reconstruction performance, their significant computational demands hinder their deployment in real-world applications, especially on resource-constrained devices. In contrast to these ANN-based methods, we introduce the use

of SNN, which offers higher energy efficiency, as a framework for achieving effective and efficient image restoration.

Deep Spiking Neural Networks. Training strategies for deep SNNs primarily fall into two categories: direct training of SNNs and ANN-SNN conversion. Despite the promising advancements in directly training SNNs using techniques such as surrogate gradients and threshold-dependent batch normalization (TDBN) for deeper architectures, these approaches still suffer from several limitations. While methods like STBP [40] and subsequent works by [13] and Fang et al. [10] have achieved success in classification tasks, they often require deep network structures (e.g., 50 layers) to perform well. This not only increases computational complexity but also contradicts the energy-efficient nature of SNNs. Furthermore, while there have been efforts to extend directly trained SNNs to regression tasks like object tracking [43, 50] and object detection [38], these approaches still rely on deep architectures to achieve satisfactory results. Song et al. [37] proposed efficient SNN architecture that has been implemented to remove rain from images. However, we tried to use it to achieve other image restoration tasks with unsatisfactory results. In contrast, our approach leverages artificial neural network feature distillation into SNNs, allowing SNNs to remain lightweight and power-efficient without sacrificing performance.

3 THE PRELIMINARIES OF SNNs

3.1 ENERGY CONSUMPTION

The number of operations is commonly used to estimate the computational energy consumption of neuromorphic hardware. In ANNs, each operation consists of multiplication and addition (MAC) involving floating-point numbers, and the computational burden is typically measured using floating-point operations (FLOPs)¹. In contrast, SNNs offer an energy-efficient alternative for neuromorphic hardware, as neurons only engage in accumulation calculations (AC) when they spike. This efficiency allows SNNs to perform computations using a similar number of synaptic operations (SyOPs), significantly reducing energy consumption compared to traditional ANN architectures. We quantify the energy consumption of vanilla SNNs as $E_{\text{SNN}} = \sum_n E_b$, for each block n :

$$E_b = T \times (fr \times E_{\text{AC}} \times \text{OP}_{\text{AC}} + E_{\text{MAC}} \times \text{OP}_{\text{MAC}}), \quad (1)$$

where T and fr represent the total time steps and the block firing rate. The blocks are normally convolutional or fully connected, and the energy consumption is determined by the number of AC and MAC operations (OP_{AC} , OP_{MAC}). In this work, we adopt the same structure of SNN and ANN to compare the energy consumption and assume that the data for various operations are 32-bit floating-point implementation in 45nm technology [12], where $E_{\text{MAC}} = 4.6pJ$ and $E_{\text{AC}} = 0.9pJ$.

3.2 STATIC IMAGE INPUTS

A common approach in SNNs for simulating pixel intensity signals in images is global encoding to generate spike signals. Taking into account the spatiotemporal properties of SNNs, we first apply direct encoding to the input degradation image to generate a sequence of spike trains, i.e. copying the single degraded image as the input for each time step $\mathbf{X} = \{\mathcal{X}_t\}_{t=1}^T$ (in this paper, we set T to 4).

4 METHOD OVERVIEW

As illustrated in Figure 2, our method comprises two primary components: an encoder-decoder framework (student network) designed to learn features for capturing information, and the distillation of knowledge from the decoders of ANNs. These parts are collaboratively worked to improve the image restoration performance of SpikerIR.

Specifically, SpikerIR incorporates a lightweight encoder designed to extract degradation features from the degraded image sequence. To balance training efficiency and performance, we introduce ‘prompts’ derived from the ANN’s network, where a prompt refers to the output of each ANN

¹<https://github.com/sovrasov/flops-counter.pytorch>

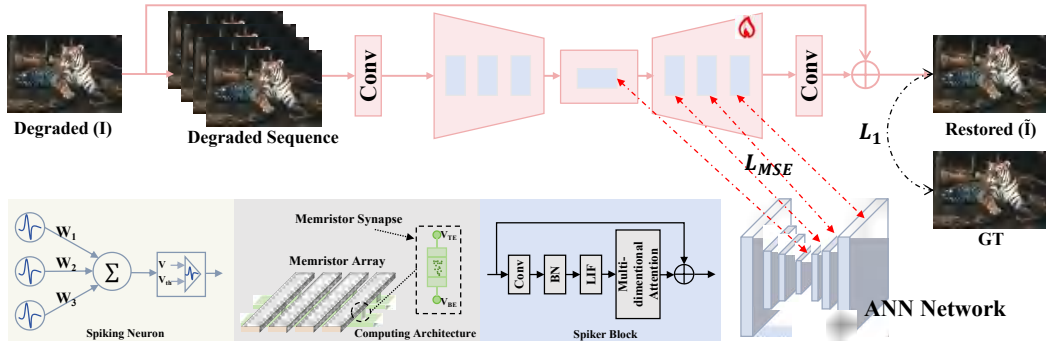


Figure 2: **Overview of our method.** SpikerIR transfers the knowledge from pre-trained ANNs’ decoders to enhance the comprehension of degradation images, helping output high-quality content features. SpikerIR is designed as an encoder-decoder architecture, which mainly contains the Spiker Block with Spike Convolution Unit and Multi-dimensional Attention.

decoder layer, which guides SpikerIR’s learning process. We employ Mean Squared Error (MSE) loss to align the outputs of each SNN decoder layer with those of the ANN, thereby facilitating learning from the ANN’s output. Furthermore, to avoid the decreasing flexibility of our SpikerIR, we leverage the L_1 loss and an FFT-based frequency loss function, which is defined as:

$$L = \|\mathbf{I}_R - \mathbf{I}_{GT}\|_1 + \lambda \|\mathcal{F}(\mathbf{I}_R) - \mathcal{F}(\mathbf{I}_{GT})\|_1, \quad (2)$$

where \mathbf{I}_R is the output of our model, \mathbf{I}_{GT} is the high-quality ground-truth image, $\|\cdot\|_1$ denotes the L_1 loss, \mathcal{F} represents the Fast Fourier transform, and λ is a weight parameter that set to be 0.1 empirically. Algorithm 1 (H-KD training strategy) procedures can be written:

Algorithm 1 the H-KD training strategy

Input:

The output of each ANN’s decoder layer \mathbf{F}_{prompt} ;
 The output of each SpikerIR’s decoder layer $\mathbf{F}_{optimize}$;
 The randomly initialized parameters \mathbf{W} of a SpikerIR.

Output:

The optimized parameters \mathbf{W}^* of SpikerIR.

$$\begin{aligned} \mathbf{F}_{prompt} &\leftarrow \{\mathbf{F}_{prompt}^1, \dots, \mathbf{F}_{prompt}^i\}; \\ \mathbf{F}_{optimize} &\leftarrow \{\mathbf{F}_{optimize}^1, \dots, \mathbf{F}_{optimize}^i\}; \\ \mathbf{W}^* &\leftarrow \gamma \arg \min_{\mathbf{F}_{optimize}} \mathcal{L}_{MSE}(\mathbf{F}_{optimize}, \mathbf{F}_{prompt}) + \arg \min_{\mathbf{W}} L_{Eq.(2)}(\mathbf{W}); \\ \text{return } \mathbf{W}^*; \end{aligned}$$

where γ represents the hyperparameter, which we set to 0.12 in this paper. It is worth noting that \mathbf{F}_{prompt} and $\mathbf{F}_{optimize}$ may not match in the size of the feature maps, which can be aligned by interpolation and pooling.

5 EXPERIMENTS

We experimentally evaluate our method on five degradation types of tasks: *motion blurry*, *hazy*, *noise*, *rainy* and *defocus blurry*. In addition, we use three existing image restoration models as teacher networks to evaluate the effectiveness of our algorithm.

5.1 IMPLEMENTATION DETAILS

We train five sets of model parameters for these five image restoration tasks within the same network framework. Our SpikerIR uses a 4-layer encoder-decoder structure, where each layer of the network is a convolutional layer and a ReLU layer. From level-1 to level-4, the number of each level SpikerIR Blocks is 2, and the number of channels is $\{48, 96, 192, 384\}$. For teacher networks, we adopt Restormer [47], PromptIR [30] and AdaIR [8] as the teacher models. We train models with AdamW

optimizer ($\beta_1=0.9$, $\beta_2=0.999$, weight decay 0.05) for 51 epochs with the initial learning rate 0.0005 gradually reduced to 0.00001 with the cosine annealing for image denoising tasks. Distinct tasks, however, were trained for different numbers of epochs to optimize performance, with the details as follows: Motion deblurring for 77 epochs, dehazing for 5 epochs, deraining for 8 epochs, and defocus deblurring for 208 epochs. We start training with patch size 64×64 and batch size 8. For data augmentation, we use horizontal and vertical flips. Two well-known metrics, Peak Signal-to-Noise Ratio (PSNR) and Structural Similarity (SSIM), are employed for quantitative comparisons. Higher values of these metrics indicate superior performance of the methods.

5.2 MAIN RESULTS

We show some quantitative and qualitative results. It is worth noting that some teacher models were not trained on the specific dataset, so the results shown may only have one SpikerIR. Some reports have three teacher models, and the results shown will have three SpikerIR's, which are represented as three student networks of teacher networks.

Image Denoising Results. We conduct denoising experiments on the synthetic benchmark dataset BSD68 [25], generated using additive white Gaussian noise. Table 1 presents the result for color image denoising. In alignment with previous methods [23, 53], we evaluated noise levels of 15, 25, and 50 during testing. Our SpikerIR achieves excellent performance for denoising tasks. Additionally, for the noise level 15 and 25, SpikerIR surpasses the teacher model Restormer. Figure 3 shows the denoised results by feature model and Our SpikerIR correspondingly for color denoising.

Table 1: **Single-image motion denoising** results. The H-KD method is applied to three different methods, i.e. Restormer, PromptIR, and AdaIR.

Method	$\sigma=15$		$\sigma=25$		$\sigma=50$	
	PSNR	SSIM	PSNR	SSIM	PSNR	SSIM
Restormer	31.96	0.900	29.52	0.884	26.62	0.688
SpikerIR	32.35	0.894	29.72	0.825	26.13	0.678
PromptIR	33.98	0.933	31.31	0.888	28.06	0.799
SpikerIR	32.48	0.898	29.70	0.829	25.59	0.642
AdaIR	34.12	0.935	31.45	0.892	28.19	0.802
SpikerIR	32.29	0.889	29.53	0.817	25.34	0.623

Image Deraining Results. The PSNR and SSIM scores across the RGB channels, as shown in Table 2, demonstrate that while our SpikerIR model achieves lower scores compared to state-of-the-art methods such as Restormer, PromptIR, and AdaIR, it is important to note that SpikerIR operates with only 1/300 of the parameter count. Our SpikerIR model adopts a similar architecture to Restormer, making Restormer a natural choice as the teacher model for comparison. Consequently, Restormer outperforms both PromptIR and AdaIR in this context, as its architectural design aligns

Table 2: **Image deraining** results. The H-KD method is applied to three different methods, i.e. Restormer, PromptIR, and AdaIR.

Method	Test100 [49]		Rain100H [45]		Rain100L [45]	
	PSNR	SSIM	PSNR	SSIM	PSNR	SSIM
Restormer [47]	32.00	0.923	31.46	0.904	38.99	0.978
SpikerIR	28.20	0.854	29.06	0.810	34.90	0.938
PromptIR	30.23	0.901	30.88	0.877	37.44	0.979
SpikerIR	30.22	0.902	30.15	0.856	33.71	0.934
AdaIR	31.79	0.979	30.99	0.889	38.02	0.981
SpikerIR	31.55	0.973	28.64	0.799	34.51	0.924

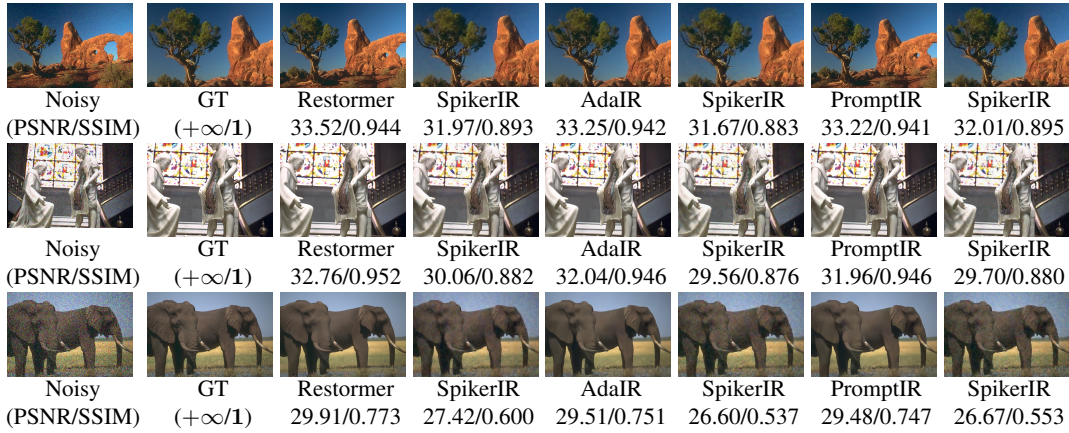


Figure 3: Visual results on **Image denoising**. Top row: the noise level is 15. Middle row: the noise level is 25. Bottom row: the noise level is 50.

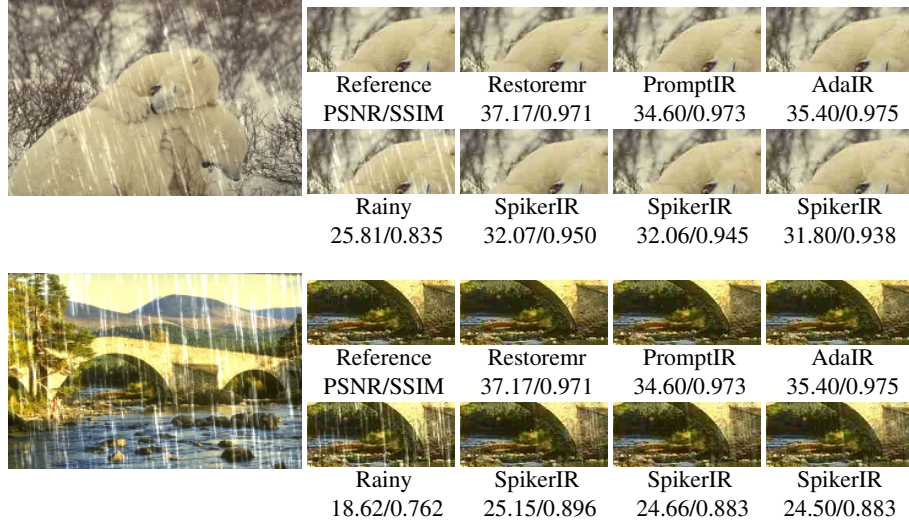


Figure 4: Single image deraining. Compared to the teacher model, our SpikerIR achieves comparable performance with significantly fewer parameters.

more closely with that of SpikerIR. This alignment enables Restormer to serve as a more effective reference for evaluating SpikerIR’s performance.

Single-image Motion Deblurring Results. Here, we use only Restormer as the teacher network, due to PromptIR and AdaIR were not evaluated poorly on this dataset. We evaluate deblurring methods both on the synthetic dataset (GoPro [27]) and the real-world datasets (RealBlur-R [35], RealBlur-J [35]). Table 3 shows that our SpikerIR receives a similar performance as the SOTA ANN models with fewer parameters and lower complexity.

Image Defocus Deblurring Results. Table 4 reports the performance of our SpikerIR on the image defocus deblurring task. Figure. 6 shows that our SpikerIR has a comparable performance in terms of deblurring quality. We also present zoomed-in cropped patches in yellow and green boxes.

Image Dehazing Results. We evaluate SpikerIR on the synthetic dataset (RESIDE/SOTS) [20]. Compared to PromptIR [30], our method generates a 0.35 dB PSNR improvement. As the Figure 7 shown, our SpikerIR is effective in removing degradations and generates images that are visually closer to the ground truth.

Table 3: Single image motion deblurring results. Our method was compared with other motion deblurring methods, and it achieved superior results on the RealBlur dataset. In addition, the number of parameters and FLOPS are much smaller than those of other models.

Method	GoPro [27]		RealBlur [35]		Params (M)	FLOPs (G))
	PSNR	SSIM	PSNR	SSIM		
MPRNet [46]	32.66	0.959	29.65	0.892	20.10	777.01
MIMO-UNet++ [4]	32.68	0.959	33.37	0.856	617.64	16.10
Restormer [47]	32.92	0.961	33.69	0.863	26.10	12.33
Stripformer [39]	33.08	0.962	25.97	0.866	20.0	170.46
SpikerIR (Ours)	29.89	0.931	30.25	0.899	0.07	0.03

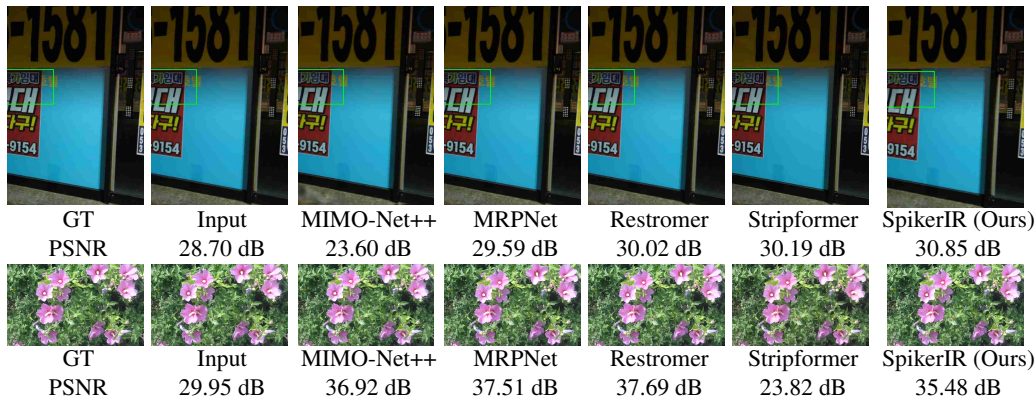


Figure 5: Visual results on image deblurring. Top row: Realworld deblurring on RealBlur dataset. Bottom row: Synthetic deblurring on Gopro Dataset.

Table 4: **Defocus deblurring** comparisons on the DPDD testset [1] (containing 37 indoor and 39 outdoor scenes). Our SpikerIR achieves excellent performance.

Method	Indoor Scenes				Outdoor Scenes				Combined			
	PSNR	SSIM	MAE	LPIPS	PSNR	SSIM	MAE	LPIPS	PSNR	SSIM	MAE	LPIPS
EBDB [15]	25.77	0.772	0.040	0.297	21.25	0.599	0.058	0.373	23.45	0.683	0.049	0.336
DMENet [17]	25.50	0.788	0.038	0.298	21.43	0.644	0.063	0.397	23.41	0.714	0.051	0.349
DPDNet [1]	26.54	0.816	0.031	0.239	22.25	0.682	0.056	0.313	24.34	0.747	0.044	0.277
IFAN [18]	28.11	0.861	0.026	0.179	22.76	0.720	0.052	0.254	25.37	0.789	0.039	0.217
Restormer [47]	28.87	0.882	0.025	0.145	23.24	0.743	0.050	0.209	25.98	0.811	0.038	0.178
SpikerIR (Ours)	26.42	0.801	0.030	0.287	21.50	0.648	0.059	0.411	23.89	0.727	0.045	0.351

Table 5: Dehazing results in the single-task setting on the SOTS-Outdoor [20] dataset.

Method	DehazeNet [3]	MSCNN [34]	AODNet [19]	EPDN [32]	FDGAN [9]	AirNet [21]	Restormer [47]	PromptIR [30]	AdaIR [8]	SpikerIR (Ours)
PSNR	22.46	22.06	20.29	22.57	23.15	23.18	30.87	31.31	31.80	31.66
SSIM	0.851	0.908	0.877	0.863	0.921	0.900	0.969	0.973	0.981	0.975

6 ABLATION STUDY AND APPLICATION

In this section, we train Gaussian color denoising models on image patches of size 64×64 for 51 epochs only. Testing is performed on BSD68 [25] dataset. Flops and energy statistics are computed on image size 256×256 . The feature models that we selected are the well-known Restormer [47], PromptIR [30], and AdaIR [8].

Impact of knowledge distillation In our H-KD method, the ANN teacher model’s decoder features are integrated into the SpikerIR to enhance intermediate-level learning. We conduct experiments to understand the impact of aligning intermediate layer features from the ANN teacher model on our SpikerIR’s performance during knowledge distillation. As the SpikerIR is the encoder-decoder

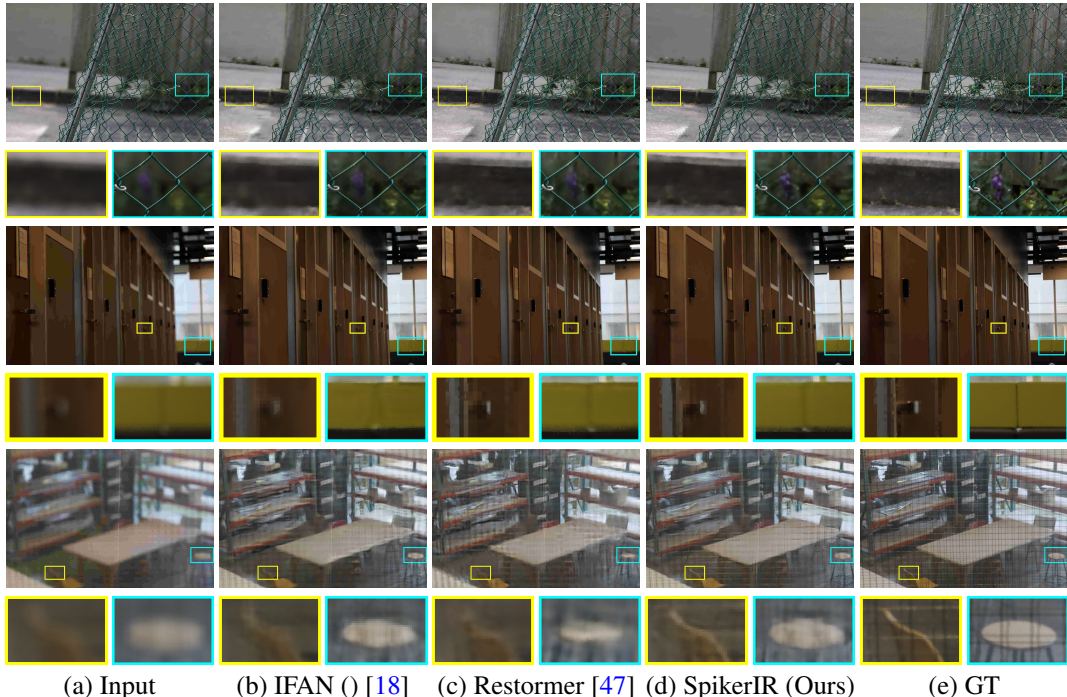


Figure 6: Qualitative comparisons with IFAN [18] and Restormer [47] on the test set of the DPDD dataset [1] for image defocus deblurring.

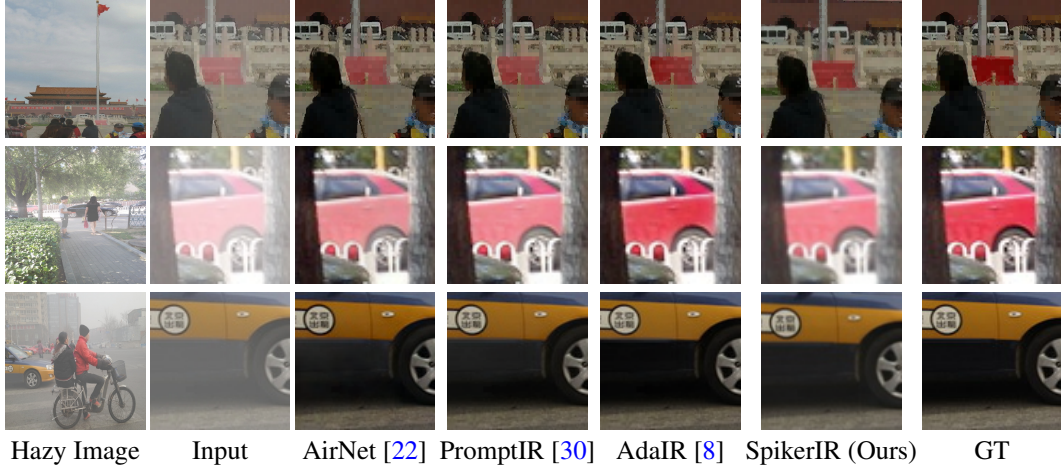


Figure 7: Image dehazing comparisons under the single task setting on SOTS [20].

framework, we perform three ablation experiments to evaluate the effects of feature constraints at different stages (stages: 1 → 7). First, we apply constraints to all the encoder and decoder layers. Second, we restrict the constraints to stages 3 → 5. Finally, we only constrain the decoder, i.e. stages 4 → 7. As shown in Table 6, when comparing learning at different feature ANNs, the SpikerIR student presents no preference for different features on denoising tasks, as they all help improve the performance.

Performance Comparison with Equivalent ANNs To highlight the efficiency of our SNN model, we compare its performance with equivalent ANNs, trained and tested using the same strategies on the BSD dataset. This comparison allows us to evaluate the energy consumption differences between the models while maintaining comparable performance. Specifically, for the ANN model, we set the number of encoder and decoder layers to match those of our SpikerIR model, and we adopt the Restormer framework for the architecture. Table 7 reports the performance, parameters and energy consumption comparison between our SNN model and the ANN model for the equivalent architecture. The evaluation models were run on a Lynxi HP300 platform to demonstrate the performance

Table 6: Ablation experiments on image denoising for learning the impact of aligning intermediate features. Without the use of distillation, there is a significant reduction in the performance of the student network.

Teacher Model	Stage 1 → 7			Stage 3 → 5			Stage 3 → 5			w/o KD		
	$\sigma=15$	$\sigma=25$	$\sigma=50$	$\sigma=15$	$\sigma=25$	$\sigma=50$	$\sigma=15$	$\sigma=25$	$\sigma=50$	$\sigma=15$	$\sigma=25$	$\sigma=50$
Restormer	32.45	29.65	25.68	31.36	29.00	25.07	32.35	29.72	26.13	30.46	27.91	22.35
PromptIR	32.50	29.61	25.04	31.98	29.15	25.35	32.48	29.70	25.59	31.44	25.00	23.26
AdaIR	32.33	29.48	25.22	31.99	29.33	25.16	32.29	29.53	25.34	31.29	25.11	22.89

Table 7: Comparison with Equivalent ANNs on image denoising.

Teature Model	Student Model	BSD68			Flops G	Params M	Energy uJ
		$\sigma=15$	$\sigma=25$	$\sigma=50$			
Restormer	SpikerIR ANN	32.45	29.65	25.68	0.07	0.03	5.232×10^4
		33.00	30.33	26.87	10.22	71.18	7.331×10^6

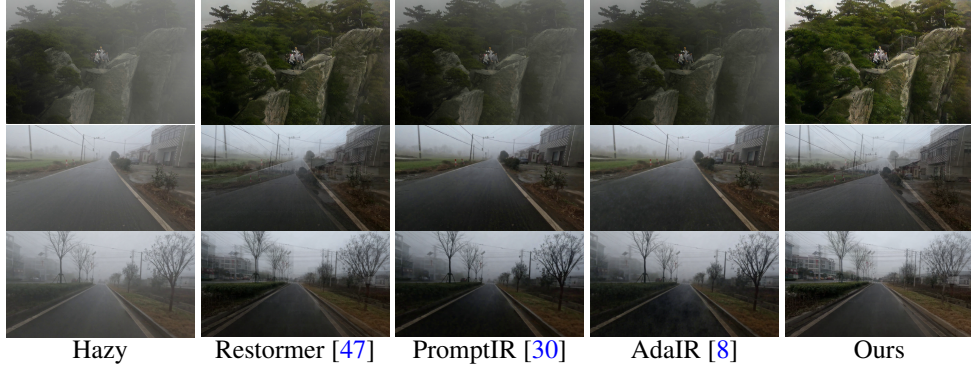


Figure 8: Real-world image dehazing results. Our method recovers images with more contrast and the haze is effectively removed.

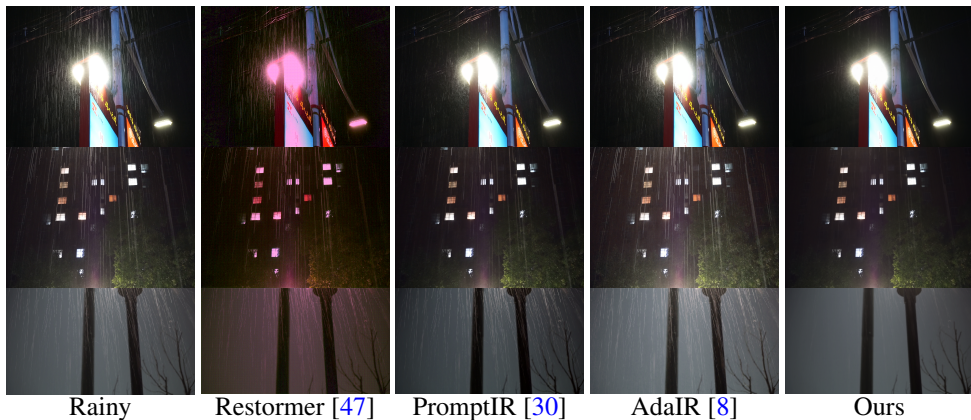


Figure 9: Real-world image deraining results. Our method effectively removes rain streaks and the glow of the wick is effectively limited.

of the models. Our model is trained on dehazing and deraining datasets with the accuracy of float16. As the Figures 9 and 8 shown, our method has better visualization, especially on real-world image dehazing tasks.

7 DISCUSSION AND LIMITATIONS

By leveraging the intermediate features from the ANN teacher model, we successfully accelerate the convergence of the SNN student (the aggregation speed of SNN models is increased by more than $5 \times$), reducing the computational burden typically associated with training SNNs. However, during our experiments, we observed two limitations related to inference and training time.

- i) The inference time in the SNN model is slower compared to its ANN counterpart (on platforms without SNN-optimized hardware, see Figure 10(b)). Although SNNs offer significant energy savings, their event-driven nature and reliance on temporal dynamics during the inference process introduce latency. Future work could explore more optimized spiking neuron models or hybrid approaches that combine the advantages of both SNNs and ANNs to improve inference speed without sacrificing energy efficiency.
- ii) Training time per epoch increases progressively as training continues, particularly in later stages (see Figure 10(a)). This phenomenon is primarily due to the complexity of gradient-based optimization in SNNs, where updating spiking neurons' membrane potentials becomes more computationally demanding as the model learns. Addressing this issue will require the development of more efficient training algorithms or hardware-accelerated solutions specifically designed for SNNs.

In addition, Figures 10(c) and 10(d) show the voltage shift of the SNN with the H-KD strategy, where the shift in Figures 10(c) is more drastic and non-sparse. A denser voltage can more effectively extract the features of an image.

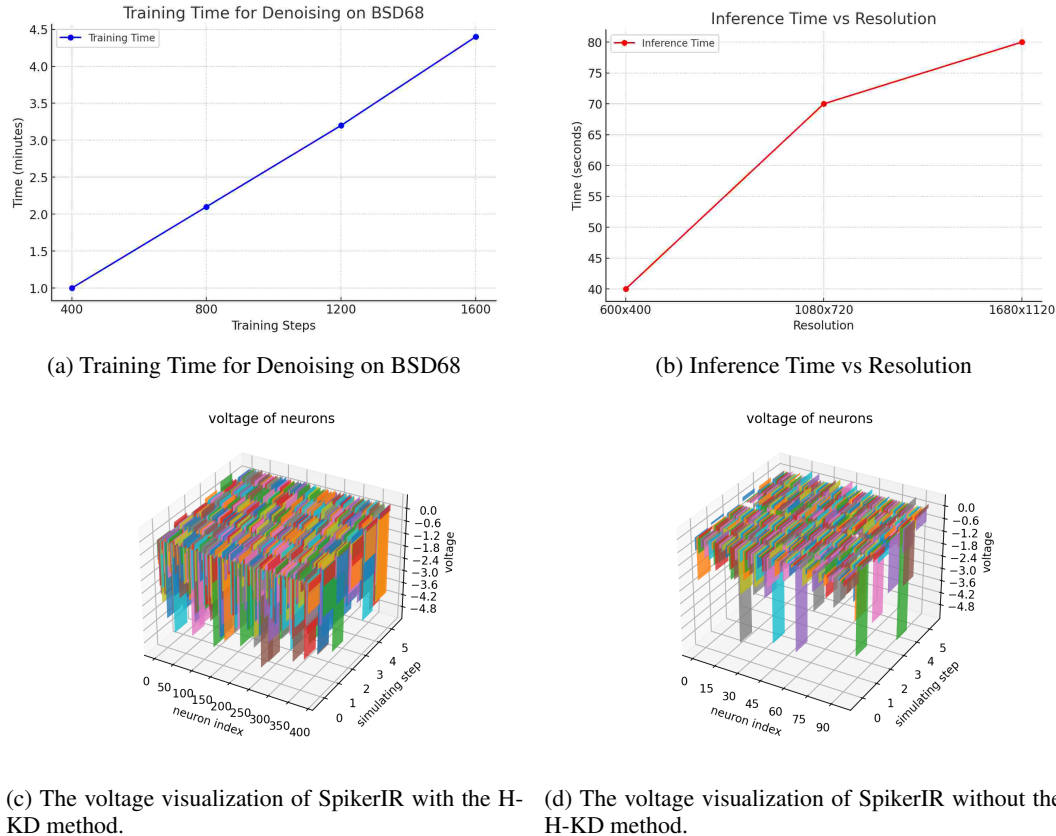


Figure 10: Comparison of training and inference times and the state of voltage membrane changes in the SNN during training.

8 CONCLUSION

In this paper, we develop an efficient, low-energy network named SpikerIR for a variety of image restoration tasks. On both GPU platforms and embedded platforms, our model demonstrates excellent performance, with clearer images than those recovered by the teacher network on some datasets. In addition, we attempted to explain the role of distillation, which acts to enable the conversion of a sparse voltage to a denser one. We also discuss some of the limitations of the model, in particular the fact that SNNs rely heavily on efficient I/O operations.

REFERENCES

- [1] Abdullah Abuolaim and Michael S Brown. Defocus deblurring using dual-pixel data. In *ECCV*, 2020. [7](#), [8](#)
- [2] Filipp Akopyan, Jun Sawada, Andrew Cassidy, Rodrigo Alvarez-Icaza, John Arthur, Paul Merolla, Nabil Imam, Yutaka Nakamura, Pallab Datta, Gi-Joon Nam, et al. Truenorth: Design and tool flow of a 65 mw 1 million neuron programmable neurosynaptic chip. *IEEE transactions on computer-aided design of integrated circuits and systems*, 34(10):1537–1557, 2015. [2](#)
- [3] Bolun Cai, Xiangmin Xu, Kui Jia, Chunmei Qing, and Dacheng Tao. Dehazenet: An end-to-end system for single image haze removal. *TIP*, 2016. [7](#)
- [4] Sung-Jin Cho, Seo-Won Ji, Jun-Pyo Hong, Seung-Won Jung, and Sung-Jea Ko. Rethinking coarse-to-fine approach in single image deblurring. In *2021 IEEE/CVF International Conference on Computer Vision (ICCV)*, pp. 4621–4630, 2021. [7](#)
- [5] Sung-Jin Cho, Seo-Won Ji, Jun-Pyo Hong, Seung-Won Jung, and Sung-Jea Ko. Rethinking coarse-to-fine approach in single image deblurring. In *ICCV*, 2021. [2](#)
- [6] Dennis V Christensen, Regina Dittmann, Bernabe Linares-Barranco, Abu Sebastian, Manuel Le Gallo, Andrea Redaelli, Stefan Slesazeck, Thomas Mikolajick, Sabina Spiga, Stephan Menzel, et al. 2022 roadmap on neuromorphic computing and engineering. *Neuromorphic Computing and Engineering*, 2(2):022501, 2022. [2](#)
- [7] Yuning Cui, Yi Tao, Wenqi Ren, and Alois Knoll. Dual-domain attention for image deblurring. In *AAAI*, 2023. [2](#)
- [8] Yuning Cui, Syed Waqas Zamir, Salman Khan, Alois Knoll, Mubarak Shah, and Fahad Shahbaz Khan. Adair: Adaptive all-in-one image restoration via frequency mining and modulation, 2024. [4](#), [7](#), [8](#), [9](#)
- [9] Yu Dong, Yihao Liu, He Zhang, Shifeng Chen, and Yu Qiao. Fd-gan: Generative adversarial networks with fusion-discriminator for single image dehazing. In *AAAI*, 2020. [7](#)
- [10] Wei Fang, Zhaofei Yu, Yanqi Chen, Tiejun Huang, Timothée Masquelier, and Yonghong Tian. Deep residual learning in spiking neural networks. *Advances in Neural Information Processing Systems*, 34:21056–21069, 2021. [3](#)
- [11] Zhiwei Hao, Jianyuan Guo, Kai Han, Yehui Tang, Han Hu, Yunhe Wang, and Chang Xu. One-for-all: Bridge the gap between heterogeneous architectures in knowledge distillation. In *Advances in Neural Information Processing Systems*, 2023. [2](#)
- [12] Mark Horowitz. 1.1 computing’s energy problem (and what we can do about it). In *2014 IEEE International Solid-State Circuits Conference Digest of Technical Papers*, pp. 10–14. IEEE, 2014. [3](#)
- [13] Yifan Hu, Lei Deng, Yujie Wu, Man Yao, and Guoqi Li. Advancing spiking neural networks towards deep residual learning. *arXiv preprint arXiv:2112.08954*, 2021. [3](#)
- [14] Kui Jiang, Zhongyuan Wang, Peng Yi, Chen Chen, Baojin Huang, Yimin Luo, Jiayi Ma, and Junjun Jiang. Multi-scale progressive fusion network for single image deraining. In *CVPR*, 2020. [2](#)
- [15] Ali Karaali and Claudio Rosito Jung. Edge-based defocus blur estimation with adaptive scale selection. *TIP*, 2017. [7](#)
- [16] Youngeun Kim and Priyadarshini Panda. Visual explanations from spiking neural networks using inter-spike intervals. *Scientific reports*, 11(1):19037, 2021. [2](#)

- [17] Junyong Lee, Sungkil Lee, Sunghyun Cho, and Seungyong Lee. Deep defocus map estimation using domain adaptation. In *CVPR*, 2019. 7
- [18] Junyong Lee, Hyeongseok Son, Jaesung Rim, Sunghyun Cho, and Seungyong Lee. Iterative filter adaptive network for single image defocus deblurring. In *CVPR*, 2021. 7, 8
- [19] Boyi Li, Xiulian Peng, Zhangyang Wang, Jizheng Xu, and Dan Feng. Aod-net: All-in-one dehazing network. In *ICCV*, 2017. 7
- [20] Boyi Li, Wenqi Ren, Dengpan Fu, Dacheng Tao, Dan Feng, Wenjun Zeng, and Zhangyang Wang. Benchmarking single-image dehazing and beyond. *TIP*, 2018. 6, 7, 8
- [21] Boyun Li, Xiao Liu, Peng Hu, Zhongqin Wu, Jiancheng Lv, and Xi Peng. All-in-one image restoration for unknown corruption. In *CVPR*, 2022. 7
- [22] Boyun Li, Xiao Liu, Peng Hu, Zhongqin Wu, Jiancheng Lv, and Xi Peng. All-in-one image restoration for unknown corruption. In *Proceedings of the IEEE/CVF conference on computer vision and pattern recognition*, pp. 17452–17462, 2022. 8
- [23] Jingyun Liang, Jie Zhang Cao, Guolei Sun, Kai Zhang, Luc Van Gool, and Radu Timofte. SwinIR: Image restoration using swin transformer. In *ICCV Workshops*, 2021. 5
- [24] Sihui Luo, Xinchao Wang, Gongfan Fang, Yao Hu, Dapeng Tao, and Mingli Song. Knowledge amalgamation from heterogeneous networks by common feature learning, 2019. 2
- [25] David Martin, Charless Fowlkes, Doron Tal, and Jitendra Malik. A database of human segmented natural images and its application to evaluating segmentation algorithms and measuring ecological statistics. In *ICCV*, 2001. 5, 7
- [26] Paul A Merolla, John V Arthur, Rodrigo Alvarez-Icaza, Andrew S Cassidy, Jun Sawada, Filipp Akopyan, Bryan L Jackson, Nabil Imam, Chen Guo, Yutaka Nakamura, et al. A million spiking-neuron integrated circuit with a scalable communication network and interface. *Science*, 345(6197):668–673, 2014. 2
- [27] Seungjun Nah, Tae Hyun Kim, and Kyoung Mu Lee. Deep multi-scale convolutional neural network for dynamic scene deblurring. In *CVPR*, 2017. 6, 7
- [28] N. Passalis, M. Tzelepi, and A. Tefas. Heterogeneous knowledge distillation using information flow modeling. In *2020 IEEE/CVF Conference on Computer Vision and Pattern Recognition (CVPR)*, pp. 2336–2345, Los Alamitos, CA, USA, jun 2020. IEEE Computer Society. 2
- [29] Chi-Sang Poon and Kuan Zhou. Neuromorphic silicon neurons and large-scale neural networks: challenges and opportunities. *Frontiers in neuroscience*, 5:108, 2011. 2
- [30] Vaishnav Potlapalli, Syed Waqas Zamir, Salman Khan, and Fahad Khan. Promptir: Prompting for all-in-one image restoration. In *Thirty-seventh Conference on Neural Information Processing Systems*, 2023. 2, 4, 6, 7, 8, 9
- [31] Xu Qin, Zhilin Wang, Yuanchao Bai, Xiaodong Xie, and Hui Zhu Jia. Ffa-net: Feature fusion attention network for single image dehazing. In *AAAI*, 2020. 2
- [32] Yanyun Qu, Yizi Chen, Jingying Huang, and Yuan Xie. Enhanced pix2pix dehazing network. In *CVPR*, 2019. 7
- [33] Dongwei Ren, Wangmeng Zuo, Qinghua Hu, Pengfei Zhu, and Deyu Meng. Progressive image deraining networks: A better and simpler baseline. In *CVPR*, 2019. 2
- [34] Wenqi Ren, Si Liu, Hua Zhang, Jinshan Pan, Xiaochun Cao, and Ming-Hsuan Yang. Single image dehazing via multi-scale convolutional neural networks. In *ECCV*, 2016. 2, 7
- [35] Jaesung Rim, Haeyun Lee, Jucheol Won, and Sunghyun Cho. Real-world blur dataset for learning and benchmarking deblurring algorithms. In *ECCV*, 2020. 6, 7
- [36] Kaushik Roy, Akhilesh Jaiswal, and Priyadarshini Panda. Towards spike-based machine intelligence with neuromorphic computing. *Nature*, 575(7784):607–617, 2019. 2
- [37] Tianyu Song, Guiyue Jin, Pengpeng Li, Kui Jiang, Xiang Chen, and Jiyu Jin. Learning a spiking neural network for efficient image deraining. In *IJCAI*, 2024. 3
- [38] Qiaoyi Su, Yuhong Chou, Yifan Hu, Jianing Li, Shijie Mei, Ziyang Zhang, and Guoqi Li. Deep directly-trained spiking neural networks for object detection. *arXiv preprint arXiv:2307.11411*, 2023. 3

- [39] Fu-Jen Tsai, Yan-Tsung Peng, Yen-Yu Lin, Chung-Chi Tsai, and Chia-Wen Lin. Stripformer: Strip transformer for fast image deblurring. In *ECCV*, 2022. 7
- [40] Yujie Wu, Lei Deng, Guoqi Li, Jun Zhu, and Luping Shi. Spatio-temporal backpropagation for training high-performance spiking neural networks. *Frontiers in neuroscience*, 12:331, 2018. 2, 3
- [41] Yujie Wu, Rong Zhao, Jun Zhu, Feng Chen, Mingkun Xu, Guoqi Li, Sen Song, Lei Deng, Guanrui Wang, Hao Zheng, et al. Brain-inspired global-local learning incorporated with neuromorphic computing. *Nature Communications*, 13(1):65, 2022. 2
- [42] Bin Xia, Yulun Zhang, Shiyin Wang, Yitong Wang, Xinglong Wu, Yapeng Tian, Wenming Yang, and Luc Van Gool. Diffir: Efficient diffusion model for image restoration. In *CVPR*, pp. 13095–13105, 2023. 2
- [43] Shuiying Xiang, Tao Zhang, Shuqing Jiang, Yanan Han, Yahui Zhang, Chenyang Du, Xingxing Guo, Licun Yu, Yuechun Shi, and Yue Hao. Spiking siamfc++: Deep spiking neural network for object tracking. *arXiv preprint arXiv:2209.12010*, 2022. 3
- [44] Qi Xu, Yixin Li, Jiangrong Shen, Jian K Liu, Huajin Tang, and Gang Pan. Constructing deep spiking neural networks from artificial neural networks with knowledge distillation. In *Proceedings of the IEEE/CVF conference on computer vision and pattern recognition*, pp. 7886–7895, 2023. 2
- [45] Wenhan Yang, Robby T Tan, Jiashi Feng, Jiaying Liu, Zongming Guo, and Shuicheng Yan. Deep joint rain detection and removal from a single image. In *CVPR*, 2017. 5
- [46] Syed Waqas Zamir, Aditya Arora, Salman Khan, Munawar Hayat, Fahad Shahbaz Khan, Ming-Hsuan Yang, and Ling Shao. Multi-stage progressive image restoration. In *CVPR*, 2021. 7
- [47] Syed Waqas Zamir, Aditya Arora, Salman Khan, Munawar Hayat, Fahad Shahbaz Khan, and Ming-Hsuan Yang. Restormer: efficient transformer for high-resolution image restoration. In *Proceedings of the IEEE/CVF Conference on Computer Vision and Pattern Recognition (CVPR)*, pp. 5728–5739, 2022. 4, 5, 7, 8, 9
- [48] Syed Waqas Zamir, Aditya Arora, Salman Khan, Munawar Hayat, Fahad Shahbaz Khan, and Ming-Hsuan Yang. Restormer: Efficient transformer for high-resolution image restoration. In *2022 IEEE/CVF Conference on Computer Vision and Pattern Recognition (CVPR)*, pp. 5718–5729, 2022. 2
- [49] He Zhang, Vishwanath Sindagi, and Vishal M Patel. Image de-raining using a conditional generative adversarial network. *TCSVT*, 2019. 5
- [50] Jiqing Zhang, Bo Dong, Haiwei Zhang, Jianchuan Ding, Felix Heide, Baocai Yin, and Xin Yang. Spiking transformers for event-based single object tracking. In *Proceedings of the IEEE/CVF Conference on Computer Vision and Pattern Recognition*, pp. 8801–8810, 2022. 3
- [51] Kai Zhang, Wangmeng Zuo, Yunjin Chen, Deyu Meng, and Lei Zhang. Beyond a gaussian denoiser: Residual learning of deep cnn for image denoising. *TIP*, 2017. 2
- [52] Kai Zhang, Wangmeng Zuo, and Lei Zhang. Ffdnet: Toward a fast and flexible solution for cnn-based image denoising. *TIP*, 2018. 2
- [53] Kai Zhang, Yawei Li, Wangmeng Zuo, Lei Zhang, Luc Van Gool, and Radu Timofte. Plug-and-play image restoration with deep denoiser prior. *TPAMI*, 2021. 5